Optics Communications 355 (2015) 586–590

Contents lists available at ScienceDirect

Optics Communications

journal homepage: www.elsevier.com/locate/optcom

Subwavelength beam focusing via multiple-metal slits arranged along a triangle surface

Sen Jia [a,b], Yiming Wu [b], Jinhai Si [a,*], Feng Chen [a], Xun Hou [a]

[a] Key Laboratory for Physical Electronics and Devices of the Ministry of Education & Shannxi Key Lab of Information Photonic Technique, School of Electronics & Information Engineering Xi'an Jiaotong University, Xianning-xilu 28, Xi'an 710049, China

[b] Optical Directional and Precise Measurement Technique Research Center, Xi'an Institute of Optics and Precision Mechanics, Chinese Academy of Sciences, Xi'an 710119, China

ARTICLE INFO

Article history:
Received 19 November 2013
Received in revised form
8 June 2015
Accepted 11 June 2015
Available online 15 June 2015

Keywords:
Surface plasmon polaritons
Subwavelength
Metal slit Focusing

ABSTRACT

A compact plasmonic structure is proposed to actualize the subwavelength beam focusing, through a metal slit array arranged along a triangular or trapezium surface profile. The incident light passes through the metal slits in the form of surface plasmon polaritons (SPPs) and then scattered into radiation fields. The constructive interference of radiation fields from individual slits with different depths and widths gives rise to beam focusing. The advantages of the proposed plasmonic lens are having a much smaller lateral dimension and broad working wavelength range. This is of importance for realizing densely integrated photonic circuits. The finite-difference time-domain (FDTD) method is employed to verify the proposed design. The simulation results indicate that the focal spot is beyond the diffraction limit.

© 2015 Elsevier B.V. All rights reserved.

1. Introduction

Surface plasmon polaritons (SPPs), electromagnetic waves coupled with collective free electron oscillations at metal/dielectric interface, play a central role in the field of nanophotonics [1–4]. The most attractive feature of SPPs is their ability of manipulating light on a subwavelength scale with resonant field enhancement [5–8]. Therefore, there is a growing interest in developing plasmonic structures. Plasmonic lenses, with the ability to focus SPPs into a spot beyond the diffraction limit, which enables various applications such as super-resolution imaging, high density optical data storage, and integrated optical circuit, have attracted an increasing research interest in recent years [9–16]. Various geometries, including circular holes with concentric grooves [9], slits flanked by linear arrays of grooves [10], metal slits with variant depths [11] or widths [13–17], and single metallic slit surrounded with grooves [17–19], have been considered to implement the focusing capability of plasmonic lenses. However, although a few excellent designs of them are capable of focusing light beyond the diffraction limit [13,14], complex structure and sophisticated parameters make them especially difficult to fabricate by using the present techniques. On the other hand, the lateral dimensions of the focusing devices are at least 4 μm [7,9,10,12–16], which is a drawback for realizing densely integrated photonic circuits. The lateral dimensions of some structures are decreased to about 2 μm [11,17]; nevertheless, the full-width at half-maximum (FWHM) of the generated focal spot is larger than the half of incident wavelength.

In this paper, we design a plasmonic structure for producing subwavelength beam focusing. The structure consists of metal slits with different widths and intervals and the slits are arranged along a triangular or trapezium surface profile. The finite-difference time-domain (FDTD) method is employed to verify the proposed designs. The simulation results indicate that the proposed lens can yield a converging beam with a focal spot size beyond the diffraction limit. Compared to other existing counterparts, our structure combines the benefits of sub-diffraction-limit focal spot size, broad working wavelength range and smaller lateral dimension.

2. Principle and design

Fig. 1(a) shows the schematic of the proposed plasmonic lens. It consists of five metallic slits symmetrically arranged along a triangular surface. The metallic slits have different widths and intervals. When incident light illuminates the bottom side of the structure, the light wave is coupled to SPP modes at the entrances of the metallic slits and transferred to the other side. The complex propagation constant β of SPP mode is determined by the

* Corresponding author.
E-mail address: jinhaisi@mail.xjtu.edu.cn (J. Si).

http://dx.doi.org/10.1016/j.optcom.2015.06.024
0030-4018/© 2015 Elsevier B.V. All rights reserved.

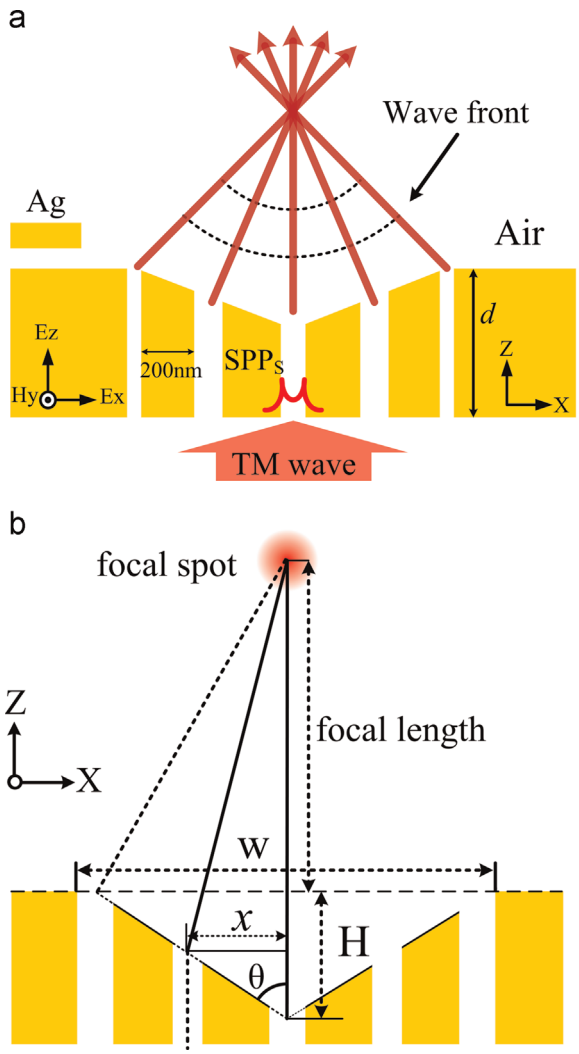

Fig. 1. (a) Schematic diagram of the proposed plasmonic lenses. A metal slit array is embedded in the metal slab with a triangular surface profile. A transverse magnetic (TM) light is incident on the bottom of the metal slab. (b) Schematic diagram of the proposed plasmonic lenses.

following equation [12]:

$$\tanh\left(\frac{w}{2}\sqrt{\beta^2 - k_0^2\varepsilon_d}\right) = \frac{-\varepsilon_d\sqrt{\beta^2 - k_0^2\varepsilon_m}}{\varepsilon_m\sqrt{\beta^2 - k_0^2\varepsilon_d}} \tag{1}$$

where k_0 is the wave vector of light in free space, ε_m and ε_d are the relative dielectric constants for the metal and the materials between slits, respectively, and w is the slit width.

The value of $\mathrm{Re}(\beta/k_0)$ represents the effective refractive index of SPPs modes in the slit and determines the phase retardation. The electric permittivity of air is 1. On the other hand, because of slits arranged along a triangular surface, the depths of slits are also different. The phase retardation $\Delta\phi$ of light passing through metal slits with variant depths can be calculated by the following equation [14]:

$$\Delta\phi = \mathrm{Re}(\beta h) + \arg\left[1 - \left(\frac{1-\beta/k_0}{1+\beta/k_0}\right)^2 \exp(2j\beta h)\right] \tag{2}$$

where h is the depth of center position of metal slit. The frequency-dependent complex relative permittivity of silver is characterized by the Drude model:

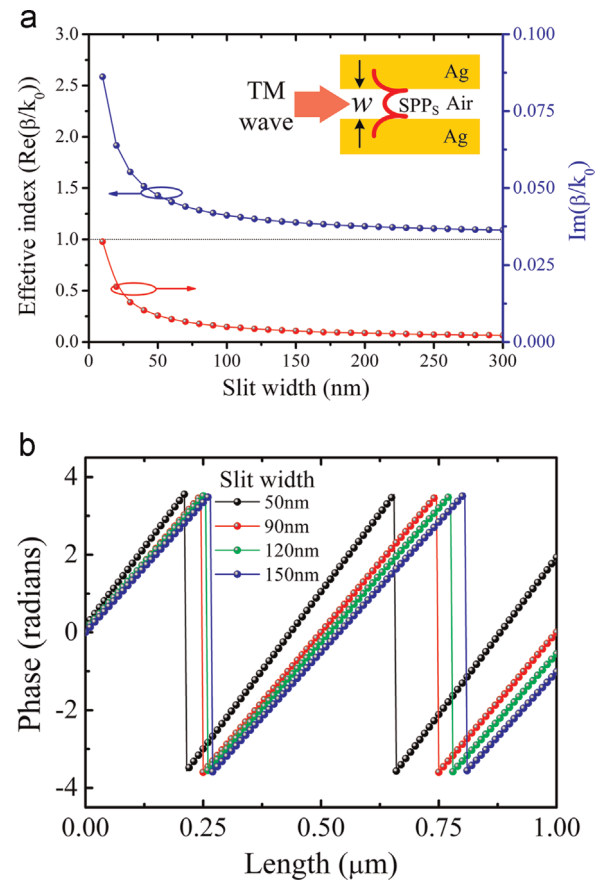

Fig. 2. (a) Dependence of effective index of SPPs in the silver slit on the slit width. The black dot line represents the value for a plane wave in air. The inset shows the schematic diagram of the metal slit structure. (b) Dependence of phase retardation of SPPs in the slit on the slit depth.

$$\varepsilon_m(\omega) = \varepsilon_\infty - \frac{\omega_p^2}{\omega(\omega + i\gamma)} \tag{3}$$

Here $\omega_p = 1.38 \times 10^{16}$ Hz is the bulk plasma frequency; $\gamma = 2.73 \times 10^{13}$ Hz is the damping frequency of the oscillations, ω is the angular frequency of the incident electromagnetic radiation, and ε_∞ stands for the dielectric constant at infinite angular frequency with a value of 3.7 [20].

Fig. 2(a) shows the dependence of effective index of SPPs mode on the slit width using silver at a wavelength of 633 nm. Fig. 2 (b) plots the phase retardation introduced by the slits with different widths and depths. The transmitted SPPs will be converted to radiating fields at the ends of metallic slits by scattering. If the parameters of metal slits such as width, depth, and interval are appropriately chosen, the radiating fields from individual metallic slits will focus at the specific point due to the constructive interference. Fig. 1(b) shows the geometric relations. Here, we define the distance from spot to the plane of metal film as the focal length. According to the geometry in Fig. 1(b), it is easy to obtain that the phase difference between the light radiated from different slits at the focusing spot position is about

$$\varphi \approx \frac{2\pi}{\lambda}\left(f + H - \sqrt{(f + H - |x|/tg\theta)^2 + x^2}\right) \tag{4}$$

where, f is the focal length, and $k_0 = 2\pi/\lambda$ is the free space wave vector of the incident light. W and H represent the width and height of the triangular $tg\theta = W/2H$. There are two notable advantages to using the triangular surface profile: This design enables decreasing the number of metal slits by constructing the

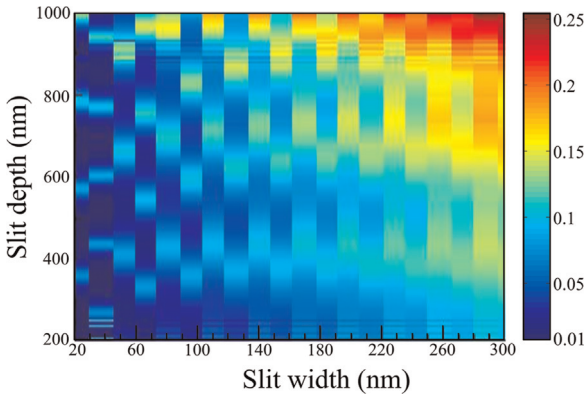

Fig. 3. Transmittance of a metallic single slit versus its width and depth at a wavelength of 633 nm.

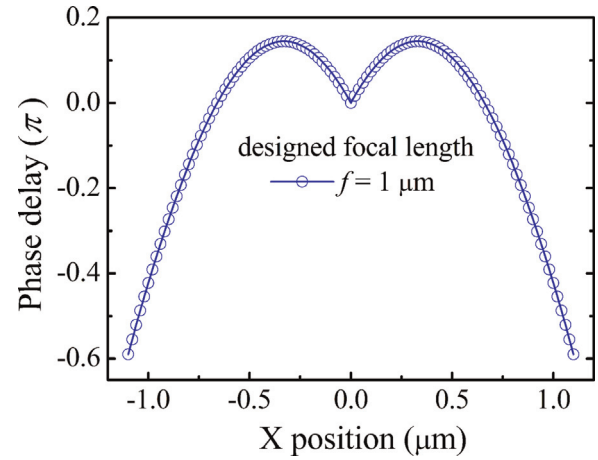

Fig. 4. The required phase delay from Eq. (4) to achieve the focal length of 1 μm.

triangular concave surface profile. Through simultaneously controlling the depth and width of slits, a required phase delay of SPPs modes for light focusing can be obtained. Second, the structure can maintain compactness in the perpendicular direction, having a large working distance. For some practical applications such as nanosensing, a large focal length is required, because the samples do not touch the surface of the plasmonic device. Although the structure has a triangular concave surface profile, it can still be seen as a planar lens.

On the other hand, owing to the radiation amplitude from slits having a marked effect on the light spot, the light transmission of a silver slit at 633 nm as a function of its width and depth is also given. Here the slit width varies from 20 to 300 nm with a 2 nm step, and slit depth changes from 200 nm to 800 nm with a step of 2 nm, respectively. Fig. 3 depicts the calculated result. From the figure, we note that the transmission of slits with a very narrow width is high and the emerging transmission peaks are discontinuous, which are attributed to the Fabry–Perot-like behavior [21]. In calculation, a power monitor is placed on the exit surface of the slit. The transmission is defined as $T=P_{out}/P_{in}$. Here, P_{in} presents the incident power at the position of the light source and P_{out} is transmission power at the position of the monitor.

3. Simulations and discussions

To demonstrate the validity of the designed structure, two-dimensional finite difference time domain (FDTD) simulation is performed. In our simulation, a mesh size of 2 nm×2 nm is employed to ensure accurate results. As a first step, we determine the geometric parameters of our proposed structure: the thickness of the Ag film is 1 μm, and the height and bottom width of surface triangular are 0.3 and 2.2 μm, respectively. Here, we choose $Z=1$ μm as the exit plane. Based on Eq. (4), for a designed focusing structure with a focal length of $f=1$ μm, the phase delay caused by the light path difference is shown in Fig. 4.

Assume that the focusing structure has five metal slits and their corresponding center positions as along the x axis can be set arbitrarily at −1.1, −0.5, 0, 0.5, and 1.1 μm. The incident light is a 633 nm plane transverse magnetic (TM) wave. The intervals between slits are much larger than the skin depth of SPPs inside the silver [22]. From Fig. 4, the phase delays from the light path difference between the center slit with other slits are 0.6, −0.15, 0, −0.15, and 0.6π from left to right, respectively. According to the geometry parameters, the depths of the slits of the designed structure are 1, 0.836, 0.7, 0.836, and 1 μm. When the width of the center slit is set to be 150 nm, it will result in a phase delay of 2.6π. Based on the calculated results shown in Fig. 2(b), a slit of width 80 nm, depth 1 μm will result in a phase delay of 4π, and a slit of width 170 nm, depth 0.836 μm will lead to a phase delay of 2.9π, which approximate the required phase retardations. Therefore, the widths of slits are set to 80, 170, 150, 170 and 80 nm from left to right.

Here, to achieve a focus spot size as small as possible, the widths of some slits in the designed device deviate from the values having maximum transmittance. For a plasmonic lens, a small focal spot size and high transmission are all important. However, our goal is to create a light spot as small size as possible, and thus transmission variation is placed in the secondary place in our design process. The normalized time-averaged magnetic field intensity $|Hy|^2$ is employed to represent the field intensity.

As shown in Fig. 5(a), a clear-cut focus appears at a short distance from the exit of the slits. The focal length is 0.645 μm, which has a deviation of 35.5% between the designed and simulated values. The reason is attributed to diffraction effect, which also plays a significant role in the focusing behavior of a lens with small size [23]. The cross section of focus spot in the x direction is given in Fig. 5(b), indicating an FWHM of 279 nm.

It should be pointed out that the width of the metal slits is at least 80 nm in our designs. The choice of parameters making the multi-slits can be fabricated by focused ion beams (FIB) in the experiment. In addition, the simulation result shows that the focal length can be controlled by only tuning the width and position of the most outboard slits. In this way the focal length is able to increase to several wavelengths. For example, when the width and position of the two slits are set to be 350 nm and ±1 μm, respectively, the focal length increases to 1.69 μm and the light spot size increases to 445 nm. Therefore, the design parameters should find a compromise between the spot size and focal length according to specific requirements.

On the other hand, most reported plasmonic focusing devices are designed for operating at a certain wavelength. However, for practical applications, it is also necessary to verify the dispersive behavior of the focusing structure. Fig. 6 shows the focusing properties of the designed structure at different incident wavelengths. Here, the simulations are carried out with the wavelength varied from 650 to 900 nm with a 50 nm step, and the other parameters are the same as those used in Fig. 5. As shown in Fig. 6, it can be seen that the focal spot size becomes large with the wavelength increasing, while the focal length gradually decreases. In addition, the simulation results show that the designed nanolens can achieve good focusing in the wavelength range of 620–910 nm.

Additionally, the focusing capability of the structure with a trapezium surface profile is also investigated. Based to the

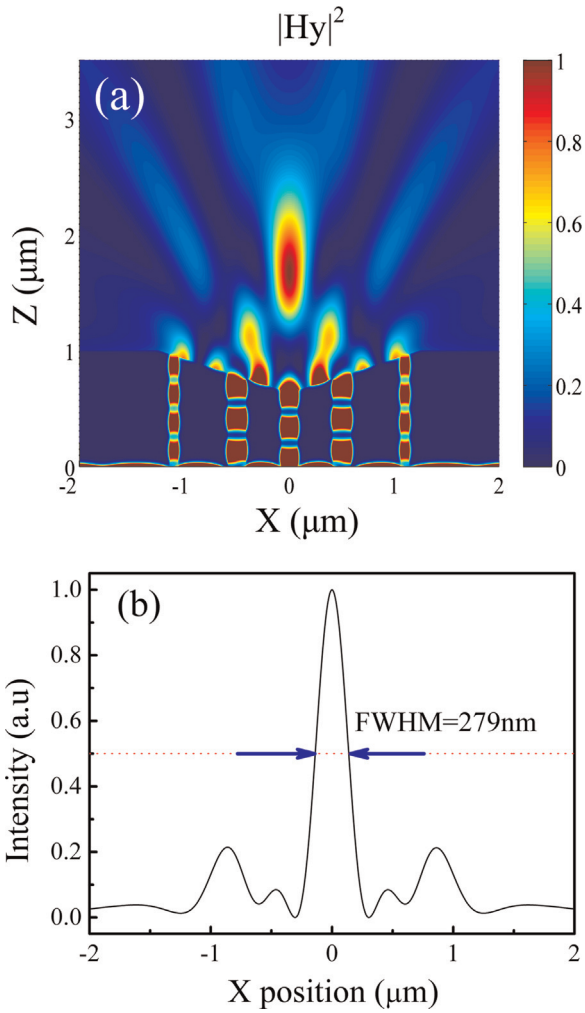

Fig. 5. (a) The normalized field intensity distribution of the transmitted lights through the plasmonic structure. (b) The cross-section at the focal point along *x* axis.

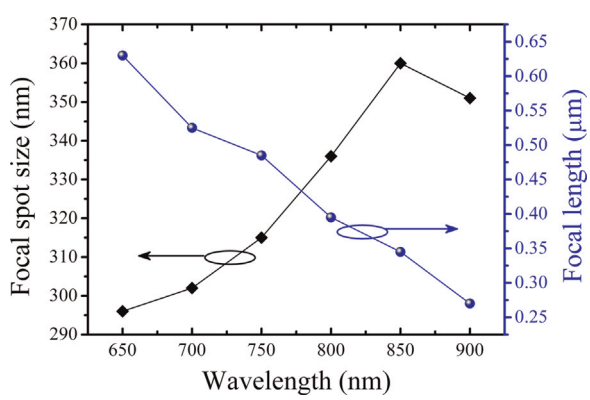

Fig. 6. Focal length and focal spot size vary with wavelength increases from 650 to 900 nm with a step of 50 nm.

designed method mentioned above, the following geometric parameters are used for the improved structure: the slits widths are 260, 220, 170, 220 and 260 nm from left to right and the corresponding center positions of slits as along the *x* axis are set at −1.15, −0.45, 0, 0.45, and 1.15 μm, respectively. Two parallel sides and the height of the trapezium surface are 0.3, 2.5, and 0.45 μm, respectively. The thickness of the Ag film keeps constant.

Fig. 7(a) shows the field intensity distribution of the

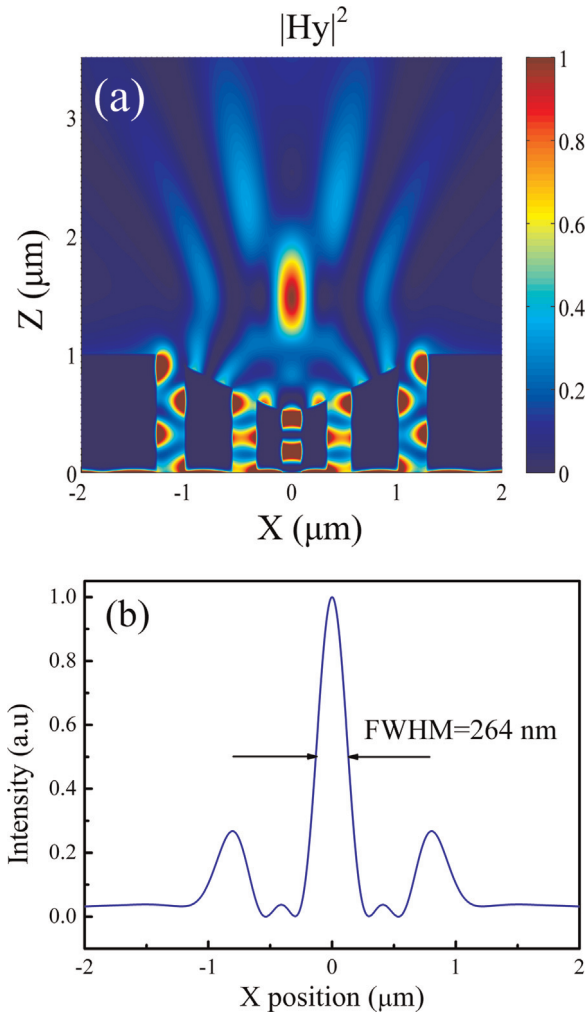

Fig. 7. (a) Normalized light field intensity distribution of the transmitted light through the metal film with trapezium surface profile. (b) The cross-section along the *x* direction at focal spot.

transmitted light at 633 nm. The cross-section of the focused beam at the focal point along the *x*-axis is shown in Fig. 7(b), where the FWHM is 264 nm. The focal length is 0.45 μm. This value is smaller than that in Fig. 5(a). It is attributed to the constructive interference between the transmitted light and the scattered SPPs from the front surface of the Ag film. In this structure, the outboard slits can support multi-order modes, owing to the large slit width. The SPPs propagating along the metal slits can be scattered by the walls of the exit slits, as shown in Fig. 7(a). Then, they will interfere with the transmitted light. Due to the focal spot being very near the front surface of the Ag film, the scattered SPPs can greatly affect the light focusing. As a result, the sides peaks in this figure are slightly higher than those in Fig. 5(b).

In all calculations above, to simplify the structure of the lens and employ the wider slits which contributes to reduce manufacturing difficulties, the metal slits are kept at five. Furthermore, we also investigate the performance of the nanolens when the number of slits increases. Here, the number of slits increases to seven. According to our designed method, the following geometric parameters are used for the improved structure: The slits widths are 260, 220, 80, 170, 80, 220 and 260 nm from left to right and the corresponding center positions of slits as along the *x*-axis are set at −1.15, −0.55, −0.25, 0, 0.25, 0.55, and 1.15 μm, respectively. The other parameters are the same as those used in Fig. 7. Fig. 8 (a) shows the field intensity distribution of the transmitted light.

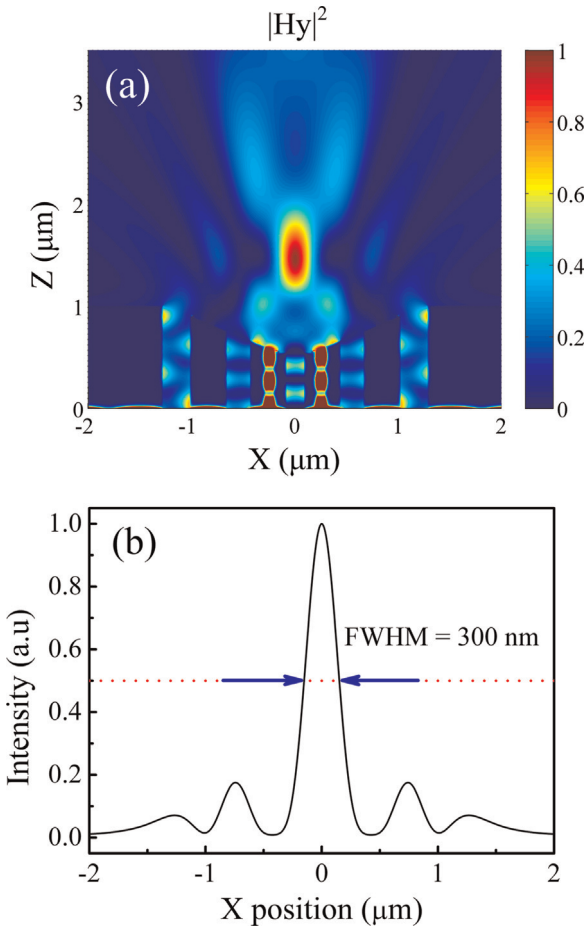

Fig. 8. (a) Light field intensity distribution of the transmitted light through the focusing structure with seven slits. (b) The intensity profile along the *x* direction at the spot.

The intensity profile at the focal point along the *x*-axis is shown in Fig. 8(b), where the FWHM is 300 nm. The focal length is about 0.455 μm. The FWHM value is larger than that in Fig. 7(a). It is attributed to the scattered SPPs from the exit surface of the Ag film.

Although the designed lens with metallic nanostructure can achieve a focal spot with a size less than a half of the illumination wavelength, it is still a difficult task to concentrate light into a volume of size far beyond the diffraction limit at visible wavelengths. Recent researches have shown that light field can be concentrated in only a few nanometers volumes by using a hybrid plasmonic waveguide or tapered metallic guiding nanostructure [8,24]. However, these devices are all working at telecommunication wavelength or mid-infrared range. Therefore, in subsequent research, we will try to design a plasmonic structure that can focus light to a spot of size far below incident wavelength at visible light.

4. Conclusion

In summary, a design of SPPs-based metal lens for subwavelength beam focusing is proposed. The advantages of our proposed plasmonic lens are smaller spot size and broad working wavelength range. FDTD simulation results show that the plasmonic structure can result in a beam focusing spot beyond the diffraction limit. These advantages promise this structure to find potential applications in integrated optical circuits, data storage, and sensors.

Acknowledgments

The authors gratefully acknowledge the financial support for this work provided by the National Basic Research Program of China (973 Program) under Grant no. 2012CB921804, and the National Natural Science Foundation of China under Grant nos. 61235003, 11404387 and 91123028.

References

[1] H. Reather, Surface Plasmons on Smooth and Rough Surfaces and on Gratings, Springer-Verlag, New York, 1988.
[2] W.L. Barnes, A. Dereux, T.W. Ebbesen, Nature 424 (2003) 824.
[3] E. Ozbay, Science 311 (2006) 189.
[4] H. Ditlbacher, J.R. Krenn, G. Schider, A. Leitner, F.R. Aussenegg, Appl. Phys. Lett. 81 (2002) 1762.
[5] A. Drezet, A.L. Stepanov, H. Ditlbacher, A. Hohenau, B. Steinberger, F. R. Aussenegg, A. Leitner, J.R. Krenn, Appl. Phys. Lett. 86 (2005) 074104.
[6] I.P. Radko, S.I. Bozhevolnyi, A.B. Evlyukhin, A. Boltasseva, Opt. Express 15 (2007) 6576.
[7] S. Griesing, A. Englisch, H. Uwe, Opt. Lett. 33 (2008) 575.
[8] R. Hao, E.F. Li, W.C. Wei, Opt. Lett. 37 (2012) 2934.
[9] L. Yin, V.K. Vlasko-Vlasov, J. Pearson, J.M. Hiller, J. Hua, U. Welp, D.E. Brown, C. W. Kimball, Nano Lett. 5 (2005) 1399.
[10] F. Lopez-Tejeria, S.G. Rodrigo, F. Martin-Moreno, Nat. Phys. 3 (2007) 324–328.
[11] Z.J. Sun, H.K. Kim, Appl. Phy. Lett. 85 (2004) 642.
[12] H.F. Shi, C.T. Wang, C.L. Du, X.G. Luo, X.C. Dong, H.T. Gao, Opt. Express 13 (2005) 6815.
[13] Q.F. Zhu, D.Y. Wang, X.H. Zheng, Y. Zhang, Appl. Opt. 50 (2011) 1879.
[14] Y.T. Yu, H. Zappe, Opt. Express 19 (2011) 9434.
[15] B. Hu, Q.J. Wang, S.W. Kok, Y. Zhang, Plasmonics (published online, November 2, 2011).
[16] Q. Chen, D.R. Cumming, Opt. Express 18 (2010) 14788.
[17] H.F. Shi, C.L. Du, X.G. Luo, Appl. Phys. Lett. 91 (2007) 093111.
[18] F.H. Hao, R. Wang, J. Wang, Plasmonics 5 (2010) 45.
[19] F.H. Hao, R. Wang, J. Wang, Opt. Express 18 (2010) 15741.
[20] X.S. Lin, X.G. Huang, Opt. Lett. 33 (2008) 2874.
[21] X.J. Jiao, P. Wang, L. Tang, Y. Lu, Q. Li, D. Zhang, P. Yao, H. Ming, J. Xie, Appl. Phys. B 80 (2005) 301.
[22] S.I. Bozhevolnyi, J. Erland, K. Leosson, P.M.W. Skovgaard, J.M. Hvam, Phys. Rev. Lett. 86 (2001) 3008.
[23] P. Ruffieux, T. Scharf, H.P. Herzig, R. Völkel, K.J. Weible, Opt. Express 14 (2006) 4687.
[24] M. Schnell, P. Alonso-Gonzalez, L. Arzubiaga, F. Casanova, E.L. Hueso, A. Chuvilin, R. Hillenbrand, Nat. Photonics 5 (2011) 283.